Nanoscale

Accepted Manuscript

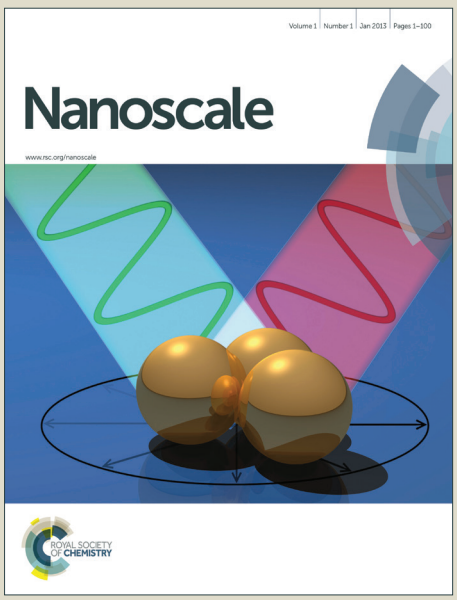

ROYAL SOCIETY OF CHEMISTRY

www.rsc.org/nanoscale

Cite this: DOI: 10.1039/c0xx00000x

www.rsc.org/xxxxxx

ARTICLE TYPE

Silica Nanonetwork Confined in Nitrogen-Doped Ordered Mesoporous Carbon Framework for High-Performance Lithium-Ion Battery Anodes

Yeru Liang,[a] Lifeng Cai,[b] Luyi Chen,[a] Xidong Lin,[a] Ruowen Fu,*[a] Mingqiu Zhang[a] and Dingcai Wu*[a]

Received (in XXX, XXX) Xth XXXXXXXXX 20XX, Accepted Xth XXXXXXXXX 20XX

DOI: 10.1039/b000000x

A new class of nitrogen-doped ordered mesoporous carbon/silica (N-OMC/SiO_2) nanocomposite was successfully fabricated *via* a multi-constituent co-assembly strategy. The N-OMC/SiO_2 nanocomposite presented a unique carbon/silica interpenetrating structure whose carbon/silica interface is highly uniform, and thus demonstrated high capacity, good cycling and excellent rate properties.

As an important class of power source devices, lithium-ion batteries (LIBs) have conquered the electronics field nowadays. With the ever-increasing energy storage demands for various technological applications, further improvement of both energy capacity and power output in LIBs is still drawing tremendous attention.[1] Optimized integration of prevalent electrode materials and innovation of their micro/nanostructures can ensure a leap forward in the performance of LIBs.[2]

Graphite has been widely used as anode material in commercial LIBs due to its good conductivity and cost effectiveness. However, its relatively low theoretical capacity (*i.e.*, 372 mAh/g) has been a major barrier in the further targeted application.[3] As alternative, silicon, stannum, stannum oxide and some metal oxides (*e.g.*, Fe_2O_3, Fe_3O_4, NiO) have been extensively exploited as anode materials with higher lithium storage capacity.[4] Among these diverse anodes, silicon has received tremendous interest for its highest theoretical capacity (approximately 4200 mAh/g).[2b, 4b, 5] However, the drastic volume variation during cycling and the tedious fabrication process of silicon have hindered its wide-spread application.

Recently, silica (SiO_2) was proposed as a promising anode material for its high theoretical capacity (approximately 1965 mAh/g) and low discharge potentials.[6] More importantly, as one of the most abundant materials in the Earth, SiO_2 is much cheaper than silicon, providing a vibrant chance to general use. Nevertheless, like silicon anode, silica is also suffering from the large volume change during lithium ions insertion/extraction, leading to severe pulverization of the electrode and thus a rapid capacity fading. In addition, the silica exhibits low intrinsic electronic conductivity, consequently delivering a poorer rate-performance than expected. To overcome these obstacles, various carbon/SiO_2 composites, whose carbon component could preserve the high electrical conductivity of the overall electrode, have been designed and fabricated by sol-gel approach, mechanical ball milling method and hydrothermal reaction.[7] Though the engineering of carbonaceous materials incorporated with silica was demonstrated to be effective ways to enhance the lithium ion storage ability, the improvement is still limited.[7c, d, 8] The main reason could be ascribed to the fact that a non-uniform interface is often formed between the silica and carbon compounds, mainly due to the intrinsical limitations of these fabrication strategies. This inevitably leads to some serious problems such as pulverization and particle aggregation. Moreover, most of the carbon/SiO_2 composites suffer from poor surface functionality. It is expected that the presence of surface chemical functionality containing heteroatoms like nitrogen can enhance the reactivity by generating additional binding sites or active sites, and hence elevate the material to a higher level of lithium ion storage capacity.[9] Therefore, construction of a uniform carbon/silica interface structure with heteroatoms doping is still a great challenge but very desirable for lithium storage. The main difficulty is the achievement of homogeneous distribution of the active silica materials confined in the carbonaceous matrix.

Herein we present a remarkable and uniform carbon/silica interface structure with nitrogen functional groups doping constructed *via* a multi-constituent co-assembly approach (Fig. 1). In this approach, phenol-formaldehyde (PF) resol is used as carbon precursor, tetraethyl orthosilicate (TEOS) as silica precursor, triblock copolymer F127 as mesopore template, and urea as nitrogen functional group source. The resulting products present a unique nitrogen-doped ordered mesoporous carbon/silica (N-OMC/SiO_2) nanocomposite architecture. Thus they combine the following dominant characteristics: i) the high conductive carbon component is well interpenetrated with silica component to form a uniform carbon/silica interface structure, thus compensating low electronic conductivity of intrinsic silica and inhibiting the significant volume expansion of silica effectively upon full lithiation; ii) the well-developed 2D hexagonal ordered mesoporous structure not only provides large enough void space to further accommodate the volume change of silica, increasing the structural integrity of the active material, but also allows for a facile lithium ion transport from the bulk electrolyte to the interior surfaces; iii) because of their valuable doping effect, nitrogen functional groups can enhance the reactivity, and hence the lithium ion storage capacity. Benefiting from such unique structural features, this class of well-defined N-OMC/SiO_2 nanocomposites can take full advantage of each constituent and hence exhibit highly impressive capacity and rate capability when used as the LIBs anode material.

Cite this: DOI: 10.1039/c0xx00000x

www.rsc.org/xxxxxx

ARTICLE TYPE

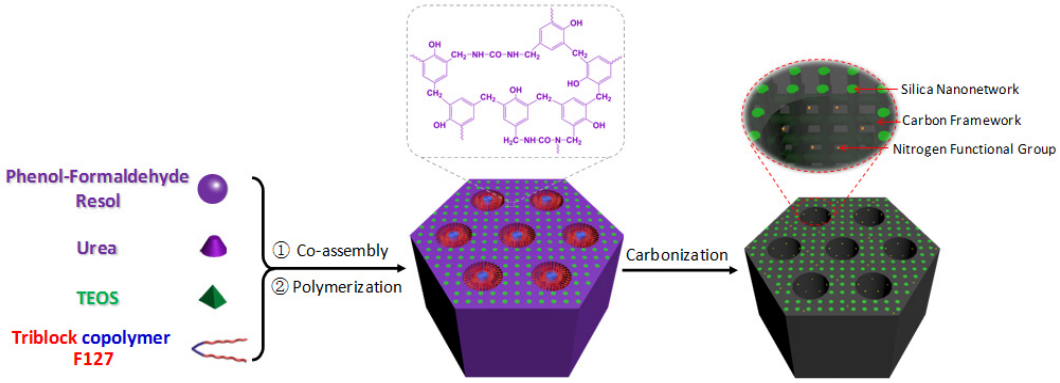

Fig. 1 Schematic diagram of the procedure for preparation of nitrogen-doped ordered mesoporous carbon/SiO_2 nanocomposite.

As schematically illustrated in Fig. 1, the N-OMC/SiO_2 nanocomposite is fabricated by using a multi-constituent co-assembly approach. Briefly, PF resol, prehydrolyzed TEOS, urea and F127 are mixed together to form a homogeneous solution. Due to its hydrophilic characteristic, urea has a good compatibility with hydrophilic PF resol and prehydrolyzed TEOS. As a result, during the multi-constituent self-assembly process, the urea species are well dispersed and coexisted in the polymer/silica composite frameworks. During the subsequent thermopolymerization of PF resol resin, the urea constituent can also react with PF resol, eventually resulting in an integral 3D thermosetting phenol-urea-formaldehyde resin framework. N-OMC/SiO_2 composite framework is obtained after the removal of the triblock copolymer F127 by carbonization at 900 ^oC in N_2 flow.

Fig. 2A displays the low-angle X-ray diffraction (XRD) patterns of the as-prepared N-OMC/SiO_2 nanocomposite. It is clearly observed that the sample possesses a well-resolved peak (10) and two weak diffraction peaks (11) and (20), suggesting the formation of highly ordered 2D hexagonal mesostructure.[10] The unit-cell parameter *a* is calculated to be 12.1 nm. More detailed structural characterization is revealed by transmission electron microscope (TEM) and scanning electron microscope (SEM) images. TEM image of N-OMC/SiO_2 nanocomposite clearly presents that uniform mesopores of as large as *ca.* 7 nm in diameter are arranged in a channel-like (Fig. 2B) and honeycomb-like (Fig. S1A) hexagonal structure. Similar results can be also found from the SEM and high angle annular dark field scanning transmission electron microscopy (HAADF-STEM) observations (Fig. 2C, 2D and S1B), further confirming the successful formation of ordered 2D hexagonal mesostructure. Estimated from TEM images, the *a* is about 12 nm for the as-obtained nanocomposite, in good accordance with the values calculated from low-angle XRD data.

The mesoporous structure is quantitatively analyzed by measurement of N_2 adsorption at 77 K (Fig. S2). The N-OMC/SiO_2 nanocomposite exhibits a type-IV isotherm with a sharp capillary condensation step at the relative pressure (P/P_0) range from 0.5 to 0.8 and an H1-type hysteresis loop, which is typical of large-pore mesoporous materials with cylindrical channel-like pores.[11] The pore sizes have a very narrow distribution with a maximum at 7.0 nm calculated from the adsorption branch based on the BJH model (see the inset in Fig. 2A), consistent with the TEM result. The BET surface area (S_{BET}) is measured to be 524 m^2/g, and the external surface area (S_{ext}) and micropore surface area (S_{mic}) are calculated *via* the t-plot method to be 368 and 139 m^2/g, respectively. The measured total pore volume (V_t) is up to 0.53 cm^3/g, most of which are contributed by the mesopore volume (Table S1).

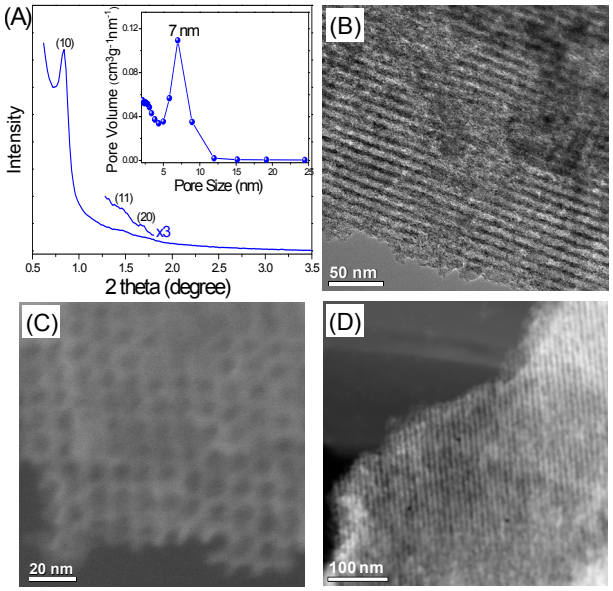

Fig. 2 (A) Low-angle XRD pattern and BJH pore size distribution (inset), (B) TEM image, (C) SEM image and (D) HAADF-STEM image of N-OMC/SiO_2 nanocomposite.

Wide-angle XRD pattern shows a distinct broad peak located in the 2θ range of 20~30^o (Fig. S3), which should be associated with the combination feature of amorphous SiO_2 and low

graphite phase. The broad and low intensity peak at *ca.* 43° ascribed to (100) plane of graphite also declares that the N-OMC/SiO_2 nanocomposite possesses a low degree of graphitization. Combined with the results from the X-ray photoelectron spectroscopy (XPS) and combustion elemental analysis, the as-constructed carbon/silica nanocomposite framework is mainly composed of carbon, oxygen, nitrogen and silicon elements (Table S2). These elements are distributed homogeneously within the nanocomposite framework, according to energy dispersive X-ray (EDX) spectroscopy mapping images for the as-obtained N-OMC/SiO_2 nanocomposite (Fig. 3). These results confirm that both carbon and silica phases are uniformly aggregated and dispersed inside pore walls on the nanoscale with a "reinforced-concrete" structure.[9b] According to the TGA analysis under air, the weight percentage of silica is estimated to be about 54 wt% (Fig. S4). The combustion analysis demonstrates that the nitrogen content is as high as about 6.3 wt% or 2.9 wt%, which is calculated based on the weight of carbon framework or the total weight of N-OMC/SiO_2 nanocomposite, respectively (Table S2). The nitrogen-containing functional groups are determined by the deconvolution of high resolution N1s XPS spectrum (Fig. S5). The N1s peak can be deconvoluted into four peaks at binding energies of 398.2, 399.7, 400.1, and 402.5 eV, which can be identified to correspond to pyridinic N (N-6), pyrrolic N (N-5), quaternary N (N-Q), and pyridine-N-oxide (N-X), respectively.[12] It can be seen from Table S3 that the percentages of N-Q and N-X in N-OMC/SiO_2 nanocomposite are relatively higher compared to that of another two types of nitrogen species. In the Fourier-transform infrared (FTIR) spectrum of N-OMC/SiO_2 nanocomposit, the peak at about 1570 cm^{-1} is attributed to the graphite-like C-N band (Fig. S6).[12c, 13]

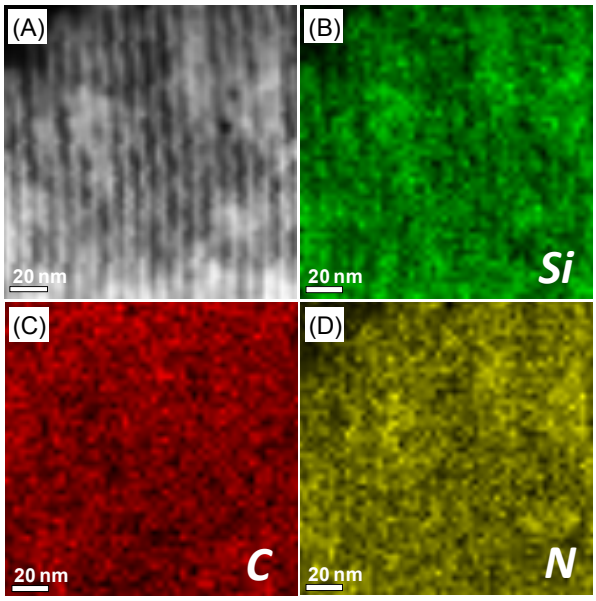

Fig. 3 (A) HAADF-STEM image of N-OMC/SiO_2 nanocomposite, and (B~D) its corresponding EDX elemental mapping: (B) silica, (C) carbon, (D) nitrogen.

N-OMC/SiO_2 nanocomposite is investigated as anode material for lithium ion batteries. The electrochemical performance of the as-obtained electrode is firstly characterized by cyclic voltammetry (CV) in coin-type half-cells (Fig. S7). There are obviously two reduction peaks in the potential of about 0.6 and 0.2 V in the first cycle. The peak at *ca.* 0.6 V can be ascribed to the electrolyte decomposition and the formation of the solid electrolyte interface (SEI) layer.[6a] Another peak at *ca.* 0.2 V is associated with the electrochemical reactions between lithium ions and SiO_2 in the nanocomposite.[14] The charge/discharge profiles in the first three cycle are shown in Fig. 4A. A plateau at *ca.* 0.6 V can be identified only in the first discharge voltage profile, which is in good agreement with the CV measurements. The initial discharge and charge capacities of N-OMC/SiO_2 nanocomposite electrode are as high as 3900 and 1996 mAh/g, respectively, giving a Coulombic efficiency of 51%. The discharge capacity of the second cycle is decreased to 1933 mAh/g. Such a large irreversible capacity (1967 mAh/g) could be attributed to the formation of SEI layer at the surface of electrodes caused by reduction of the electrolyte, and to the irreversible electrochemical reactions caused by insertion of lithium ions into special positions in the carbon/SiO_2 framework. In the subsequent charge/discharge process, the capacity becomes more stable and reversible (Fig. 4A).

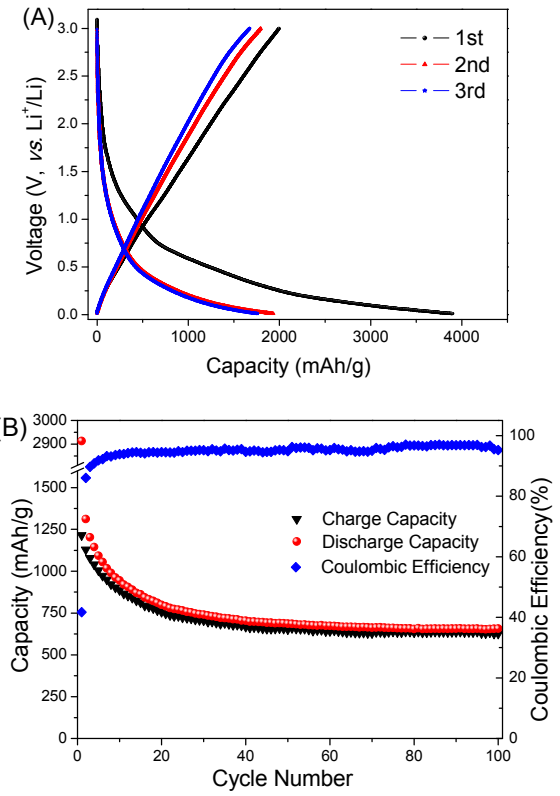

Fig. 4 Electrochemical performance of the N-OMC/SiO_2 nanocomposite electrode: (A) charge/discharge profiles in the first three cycle measured at 100 mA/g, and (B) cyclability and Coulombic efficiency at 200 mA/g.

The cycling performance of N-OMC/SiO_2 nanocomposite is evaluated at a current density of 100 mA/g in the voltage range of 0.01~3 V. As shown in Fig. S8, the N-OMC/SiO_2 nanocomposite exhibits a remarkable cycling performance. Although the capacity decays in the initial ten cycles, the discharge capacity can retain a large value of 740 mAh/g even after 50 cycles, which is about twice as high as the theoretical value of graphite. For

comparison, the lithium ion storage capacity of an ordered mesoporous carbon/silica (OMC/SiO_2) nanocomposite without nitrogen-doping is also investigated. It is found that N-OMC/SiO_2 possesses superior specific capacity to OMC/SiO_2 during charge/discharge cycling process (Fig. S9), demonstrating the important role of nitrogen functional group in improving the electrochemical performance of ordered mesoporous carbon/silica framework.

In addition, the N-OMC/SiO_2 nanocomposite also displays outstanding performance at a larger current density. As shown in Fig. 4B, the discharge capacity still remains 800 mAh/g after 20 cycles at 200 mA/g, which is comparable to that at 100 mA/g (876 mAh/g). The initial Coulombic efficiency of 42% increases dramatically upon cycling, reaching over 90% after 3 cycles and basically staying constant at 95% after 20 cycles. Notably, the N-OMC/SiO_2 nanocomposite anode still shows high lithium ion storage even at relatively high charge/discharge rates. To the best of our knowledge, there have been rare reports about SiO_2-based material anodes simultaneously possessing such exceptionally high lithium ion storage capacity and excellent cycling stability (Table S4).

The good rate capacity of the N-OMC/SiO_2 anode material is further evaluated. The as-obtained cell is firstly cycled at 50 mA/g for 10 cycles, followed by cycling with a stepwise increase of the charge/discharge rates to as high as 5000 mA/g (Fig. 5). The reversible discharge capacities of 778 mAh/g at the rate of 100 mA/g, 598 mAh/g at 150 mA/g, 490 mAh/g at 250 mA/g, 372 mAh/g at 500 mA/g, and 289 mAh/g at 1000 mA/g can be achieved, respectively. When the charge/discharge rate is recovered to 100 mA/g after cycling at different rates, the N-OMC/SiO_2 nanocomposite anode still possess a specific capacity recovered to *ca.* 650 mAh/g, demonstrating stable cycling and good rate performance.

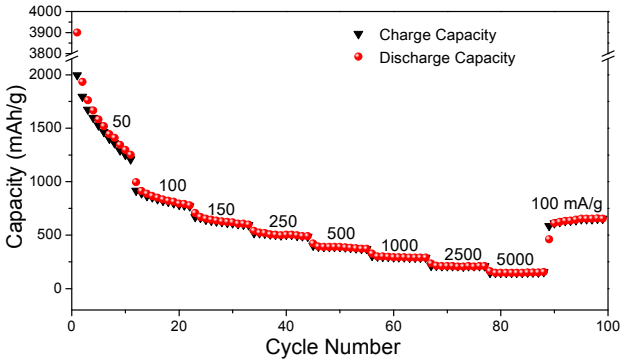

Fig. 5 Capacity over cycling of the N-OMC/SiO_2 nanocomposite electrode at various current densities.

The high capacity, good cyclic performance and excellent rate properties make the N-OMC/SiO_2 nanocomposite a promising candidate as anode material for high-performance LIBs. Such pronounced electrochemical performance are mainly ascribed to its unique and advanced nanocomposite structure, as shown in Fig. 1. First of all, the silica nanonetwork homogeneously confined inside the carbon walls can inhibit the significant volume expansion upon full lithiation, and simultaneously compensate low electronic conductivity of intrinsic silica. Moreover, the robust ordered mesoporous structure with a size as large as 7 nm can not only provide large enough void space to buffer the volume change of silica, but also offer facile lithium ion transport from the bulk electrolyte to the interior surfaces. In addition, the carbon constituent can contribute to the total lithium ion storage capacity to a certain extent,[15] and its nitrogen functional groups can further enhance the reactivity by generating additional binding sites or active sites,[9a-e] leading to an improved lithium ion storage performance.

In conclusion, we have successfully prepared a new class of N-OMC/SiO_2 *via* a resol resin/TEOS/triblock copolymer/urea multi-constituent co-assembly strategy. The resultant products with a unique carbon/silica interpenetrating network structure possess large mesopore size of *ca.* 7 nm, high surface area of 524 m^2/g and large pore volume of 0.53 cm^3/g. The high effectiveness of the as-constructed silica/carbon interface architecture was demonstrated in terms of high capacity, good cycling and excellent rate properties of N-OMC/SiO_2 during the lithium ions insertion/extraction reaction process. We hope that such a silica nanonetwork confined in nitrogen-doped ordered mesoporous carbon wall will be versatile and could be generally extended to a wide range of carbon and other alloy-type electrode materials (*e.g.*, Fe_3O_4, TiO_2), which commonly suffer from large volume change during electrochemical operation.

Acknowledgments

The projects of Guangdong Natural Science Funds for Distinguished Young Scholar (S2013050014408), NSFC (51422307, 51372280, 51173213, 51172290, 51232005), China Postdoctoral Science Foundation (2014M560686), Program for New Century Excellent Talents in University (NCET-12-0572), Program for Pearl River New Star of Science and Technology in Guangzhou (2013J2200015) and National Key Basic Research Program of China (2014CB932402) are acknowledged for funding.

Notes and references

[a] *Materials Science Institute, PCFM Lab and GDHPPC Lab, School of Chemistry and Chemical Engineering, Sun Yat-sen University, Guangzhou, 510275, P. R. China.*
Fax: +86-020-84112759; Tel: +86-020-84112759;
E-mail: wudc@mail.sysu.edu.cn; cesfrw@mail.sysu.edu.cn
[b] *College of Environmental and Biological Engineering, Putian University, Putian 351100, P. R. China*

[1] Electronic Supplementary Information (ESI) available: Experimental details, Table S1~S4 and Fig. S1-S9. See DOI: 10.1039/b000000x/

[2] Y. R. Liang and L. F. Cai contributed equally to this work.

1. (a)M. Armand and J. M. Tarascon, *Nature*, 2008, **451**, 652; (b)B. Kang and G. Ceder, *Nature*, 2009, **458**, 190; (c)Y. Li, Z. Fu and B. Su, *Adv. Funct. Mater.* , 2012, **22**, 4634; (d)D. S. Su and R. Schlogl, *Chemsuschem*, 2010, **3**, 136; (e)C. Liu, F. Li, L. P. Ma and H. M. Cheng, *Adv. Mater.* , 2010, **22**, E28.
2. (a)H. Wu, G. Yu, L. Pan, N. Liu, M. T. McDowell, Z. Bao and Y. Cui, *Nat. Commun.*, 2013, **4**; (b)D. S. Jung, M. H. Ryou, Y. J. Sung, S. B. Park and J. W. Choi, *PNAS* 2013, **110**, 12229.
3. L. Qie, W. M. Chen, Z. H. Wang, Q. G. Shao, X. Li, L. X. Yuan, X. L. Hu, W. X. Zhang and Y. H. Huang, *Adv. Mater.* , 2012, **24**, 2047.
4. (a)Y.-Y. Hu, Z. Liu, K.W. Nam, O. J. Borkiewicz, J. Cheng, X. Hua, M. T. Dunstan, X. Yu, K. M. Wiaderek, L.S. Du, K. W. Chapman, P. J. Chupas, X.Q. Yang and C. P. Grey, *Nat. Mater.* , 2013, **12**, 1130; (b)K. Ogata, E. Salager, C. J. Kerr, A. E. Fraser, C. Ducati, A. J. Morris, S.

Hofmann and C. P. Grey, *Nat. Commun.*, 2014, **5**, 11; (c)H. Nishihara and T. Kyotani, *Adv. Mater.* , 2012, **24**, 4473; (d)N. S. Choi, Z. Chen, S. A. Freunberger, X. Ji, Y. K. Sun, K. Amine, G. Yushin, L. F. Nazar, J. Cho and P. G. Bruce, *Angew. Chem. Int. Ed.* , 2012, **51**, 9994.

5. N. Liu, Z. Lu, J. Zhao, M. T. McDowell, H.W. Lee, W. Zhao and Y. Cui, *Nat. Nanotechnol.* , 2014, **9**, 187.
6. (a)N. Yan, F. Wang, H. Zhong, Y. Li, Y. Wang, L. Hu and Q. Chen, *Sci Rep*, 2013, **3**, 1568; (b)W.S. Chang, C.M. Park, J.H. Kim, Y.U. Kim, G. Jeong and H.-J. Sohn, *Energy Environ. Sci.* , 2012, **5**, 6895; (c)Z. Favors, W. Wang, H. H. Bay, A. George, M. Ozkan and C. S. Ozkan, *Sci. Rep.*, 2014, **4**, 1; (d)J. Tu, Y. Yuan, P. Zhan, H. Jiao, X. Wang, H. Zhu and S. Jiao, *J. Phys. Chem. C* 2014, **118**, 7357; (e)X. Li, A. Dhanabalan, X. Meng, L. Gu, X. Sun and C. Wang, *Micropor. Mesopor. Mater.*, 2012, **151**, 488; (f)M. Sasidharan, D. Liu, N. Gunawardhana, M. Yoshio and K. Nakashima, *J. Mater. Chem.* , 2011, **21**, 13881.
7. (a)M. Li, J. Li, K. Li, Y. Zhao, Y. Zhang, D. Gosselink and P. Chen, *J. Power Sources* 2013, **240**, 659; (b)B. Guo, J. Shu, Z. Wang, H. Yang, L. Shi, Y. Liu and L. Chen, *Electrochem. Commun.* , 2008, **10**, 1876; (c)P. Lv, H. Zhao, J. Wang, X. Liu, T. Zhang and Q. Xia, *J. Power Sources* 2013, **237**, 291; (d)J.J. Zhang, Z. Wei, T. Huang, Z.L. Liu and A.S. Yu, *J. Mater. Chem. A*, 2013, **1**, 7360.
8. (a)J. Wang, H. Zhao, J. He, C. Wang and J. Wang, *J. Power Sources* 2011, **196**, 4811; (b)J. Shu, R. Ma, M. Shui, D. Wang, N. Long, Y. Ren, R. Zhang, J. Yao, X. Mao, W. Zheng and S. Gao, *RSC Advances*, 2012, **2**, 5806.
9. (a)Z. Li, Z. Xu, X. Tan, H. Wang, C. M. B. Holt, T. Stephenson, B. C. Olsen and D. Mitlin, *Energy Environ. Sci.* , 2013, **6**, 871; (b)Z.-S. Wu, W. Ren, L. Xu, F. Li and H.M. Cheng, *ACS Nano*, 2011, **5**, 5463; (c)X.G. Sun, X. Wang, R. T. Mayes and S. Dai, *Chemsuschem*, 2012, **5**, 2079; (d)L. Qie, W.M. Chen, Z.H. Wang, Q.G. Shao, X. Li, L.X. Yuan, X.L. Hu, W.X. Zhang and Y.H. Huang, *Adv. Mater.* , 2012, **24**, 2047; (e)F. Su, C. K. Poh, J. S. Chen, G. Xu, D. Wang, Q. Li, J. Lin and X. W. Lou, *Energy Environ. Sci.* , 2011, **4**, 717; (f)Y. Liang, D. Wu and R. Fu, *Sci. Rep.*, 2013, **3**; (g)H. Liu, Z. Li, Y. Liang, R. Fu and D. Wu, *Carbon*, 2015, **84**, 419.
10. (a)Y. Fang, Y. Lv, R. Che, H. Wu, X. Zhang, D. Gu, G. Zheng and D. Zhao, *J. Am. Chem. Soc.* , 2013, **135**, 1524; (b)R. Liu, Y. Shi, Y. Wan, Y. Meng, F. Zhang, D. Gu, Z. Chen, B. Tu and D. Zhao, *J. Am. Chem. Soc.* , 2006, **128**, 11652; (c)Y. Meng, D. Gu, F. Zhang, Y. Shi, H. Yang, Z. Li, C. Yu, B. Tu and D. Zhao, *Angew. Chem. Int. Ed.* , 2005, **44**, 7053; (d)Y. Liang, D. Wu and R. Fu, *Langmuir*, 2009, **25**, 7783.
11. (a)C. D. Liang, Z. J. Li and S. Dai, *Angew. Chem. Int. Ed.* , 2008, **47**, 3696; (b)D. Wu, Y. Liang, X. Yang, C. Zou, Z. Li, G. Lv, X. Zeng and R. Fu, *Langmuir*, 2008, **24**, 2967.
12. (a)D. Hulicova-Jurcakova, M. Seredych, G. Q. Lu and T. J. Bandosz, *Adv. Funct. Mater.* , 2009, **19**, 438; (b)Y. Liang, H. Liu, Z. Li, R. Fu and D. Wu, *J. Mater. Chem. A*, 2013, **1**, 15207; (c)G. Xu, B. Ding, P. Nie, L. Shen, J. Wang and X. Zhang, *Chemistry-a European Journal*, 2013, **19**, 12306.
13. S. N. Talapaneni, G. P. Mane, A. Mano, C. Anand, D. S. Dhawale, T. Mori and A. Vinu, *Chemsuschem*, 2012, **5**, 700.
14. Y. Yao, J. Zhang, L. Xue, T. Huang and A. Yu, *J. Power Sources* 2011, **196**, 10240.
15. B. Guo, X. Wang, P. F. Fulvio, M. Chi, S. M. Mahurin, X.-G. Sun and S. Dai, *Adv. Mater.* , 2011, **23**, 4661.